RESEARCH ARTICLE

Macromolecular Rapid Communications
www.mrc-journal.de

Block Copolymers of Polyolefins with Polyacrylates: Analyzing and Improving the Blocking Efficiencies Using MILRad/ATRP Approach

*Khidong Kim, Dung Nguyen, Jacobo Strong, Sajjad Dadashi-Silab, Mingkang Sun, Huong Dau, Anthony Keyes, Rongguan Yin, Eva Harth, and Krzysztof Matyjaszewski**

Despite their industrial ubiquity, polyolefin-polyacrylate block copolymers are challenging to synthesize due to the distinct polymerization pathways necessary for respective blocks. This study utilizes MILRad, metal–organic insertion light-initiated radical polymerization, to synthesize polyolefin-*b*-poly(methyl acrylate) copolymer by combining palladium-catalyzed insertion–coordination polymerization and atom transfer radical polymerization (ATRP). Brookhart-type Pd complexes used for the living polymerization of olefins are homolytically cleaved by blue-light irradiation, generating polyolefin-based macroradicals, which are trapped with functional nitroxide derivatives forming ATRP macroinitiators. ATRP in the presence of Cu(0), that is, supplemental activators and reducing agents , is used to polymerize methyl acrylate. An increase in the functionalization efficiency of up to 71% is demonstrated in this study by modifying the light source and optimizing the radical trapping condition. Regardless of the radical trapping efficiency, essentially quantitative chain extension of polyolefin-Br macroinitiator with acrylates is consistently demonstrated, indicating successful second block formation.

1. Introduction

Polyolefins (POs) currently form the largest class of synthetic polymers due to low-cost monomers as well as low-cost production.[1,2] Polyethylene and polypropylene are photo and chemically stable, and highly durable. Furthermore, the physical and chemical properties can be finely tuned using other alkenes as comonomers.

Functionalized POs—block copolymers (BCPs) comprised of PO block and the polar vinyl block—are especially attractive. They may serve as a bridge that connects POs to a wide range of functionalities while conserving their advantageous chemical, physical, and thermal properties.[3] However, the preparation of such materials is challenging due to the inherent differences in the reactivities of olefinic and polar vinyl monomers. Ziegler–Natta, metallocene-based catalysts[4–9] and Brookhart-type catalysts[10,11] allow access to high molecular weight POs via coordination–insertion polymerization and chain-walking processes.[10–12] On the other hand, radical-stabilizing functionality allows polar vinyl monomers to be polymerized via controlled radical polymerization, such as atom transfer radical polymerization, ATRP.[13–16]

ATRP, as one of the major types of reversible deactivation radical polymerization (RDRP), allows polymerization with high chain end functionality, low dispersity, and controlled growth since its introduction nearly 30 years ago.[15] ATRP has continued to develop toward higher efficiency, lower environmental impact, and diversification in mechanistic approaches.[17–19] Such advancements included iron-catalyzed ATRP[20–22] metal-free ATRP,[23] and low-ppm,[24] regenerative ATRP methods.[18,24] Improved ATRP techniques were introduced, including initiators for continuous activator regeneration (ICAR)[17] ATRP, photoATRP,[25,26] activators regenerated by electron transfer ATRP,[27,28] and supplemental activators and reducing agents (SARA) ATRP.[29–31]

Both coordination–insertion polymerization and ATRP are highly efficient and commercially successful strategies—for respective monomers. The polymerization approaches to POs and polar vinyl polymers are not interchangeable. Organometallic procedures are less suitable for the polymerization of polar monomers;[32] acrylic monomers poison the transition-metal catalysts, effectively halting the polymerization process.[33] Vice versa, olefinic monomers are not compatible with RDRP as

K. Kim, S. Dadashi-Silab, M. Sun, R. Yin, K. Matyjaszewski
Department of Chemistry
Carnegie Mellon University
Pittsburgh, PA 15213, USA
E-mail: km3b@andrew.cmu.edu

D. Nguyen, J. Strong, H. Dau, A. Keyes, E. Harth
Department of Chemistry
Center of Excellence in Polymer Chemistry (CEPC)
University of Houston
Houston, TX 77204, USA

The ORCID identification number(s) for the author(s) of this article can be found under https://doi.org/10.1002/marc.202300675

DOI: 10.1002/marc.202300675

the active centers cannot be sufficiently stabilized in controlled radical polymerizations.[34] Using Brookhart-type catalysts, the chain-walking process allows the incorporation of a single vinyl monomer preferentially at the end of the PO branch.[11,35] However, continuous vinyl monomer polymerization is not possible, hindering the synthesis of polyolefin–polar BCPs.[36,37]

Traditional approaches to prepare PO-polar block copolymer require harsh conditions and multiple-step procedures.[38] Copolymerization of functionalized reagents may be accompanied by side reactions and a low level of incorporations.[39] Previous studies by Harth et al.,[32,40] shifted from such a paradigm and demonstrated the efficient combination of different polymerization methods by using a single catalyst approach.[40] MILRad, metal–organic insertion light-initiated radical polymerization, represents a fusion of two polymerization methods.[32,40,41]

The first step of the MILRad approach involves the preparation of a highly branched polyolefin block via coordination–insertion polymerization with a palladium–centered Brookhart–type catalyst.[8,42] The polymerization was retarded significantly upon the addition of methyl acrylate, forming a stable six-membered ring macrochelate. The presence of acetonitrile or methyl acrylate promotes the opening of the chelate, allowing the palladium chain-walking to the α-carbon, which is necessary for the subsequent homolytic cleavage of Pd—C bond and formation of PE-macroradicals.[32]

Such PE-macroradicals initiated the free radical polymerization (FRP) of acrylates in the case of the original MILRad polymerization approach. FRP yielded a radical primarily at the α-position to the carbonyl, followed by the addition of acrylates. Such prototypical MILRad strategy,[32] however, had limited control, typical for free radical polymerization. Furthermore, the scope of monomers was also limited excluding vinyl acetate or acrylamide monomers.[40]

Later works of MILRad, based on the tandem living insertion strategy,[40,41] linked coordination polymerization with RDRP approaches, instead of FRP. The PO-based macroradical formed from homolytic cleavage was captured via radical trapping with nitroxides such as TEMPO (2,2,6,6-tetramethylpiperidin-1-yl)oxyl), TIPNO (2,2,5-trimethyl-4-phenyl -3-azahexane-3-nitroxide), and TEMPO-Br (1-oxyl-(2,2,6,6-tetramethylpiperidine)−4-yl α-bromoisobutyrate).[41] The tandem polymerization achieved through MILRad demonstrated the usage of nitroxide derivatives as a means to install functional polymerization handles via radical trapping.[41] The installed terminal α-bromoisobutyrate converted the PO chain ends to macroinitiators for ATRP, enabling block copolymerization. This is an example of efficient end functionalization to link polyolefins with a wide array of blocks.[43]

Despite being an efficient pathway to install a radical polymerization handle, the trapping efficiencies of TEMPO-Br were limited.[41] Another portion of PO chains cleaved from macrochelates underwent elimination to form internal and terminal unsaturated PO chains (**Figure 1**). Because of the limited chain-end functionalization achieved with TEMPO-Br radical traps and the inability of the subsequent unfunctionalized polyethylene to undergo ATRP, this study focused on quantifying the initiation efficiency of the macroinitiators.

Furthermore, this study also explored the strategies to improve the radical trapping efficiency using TEMPO-Br as the nitroxide trap. The ^{1}H NMR analysis showed that the trapping efficiency was improved from ≈50% to >70% by changing the light intensity. Furthermore, this study also demonstrated almost quantitative initiation of macroinitiators via SARA ATRP. High initiation efficiency indicated that the presence of excess unfunctionalized PO chains did not limit the activation of macroinitiators or the polymerization of acrylates.

2. Results and Discussion

As shown in Figure 1 (Bottom), the MILRad functionalization technique with RDRP provided a smooth transition from the coordination–insertion polymerization to ATRP.[41] Palladium-based Brookhart-type catalyst 1A was employed to form amorphous polyethylenes via chain-walking under high pressure (Figure S1, Supporting Information).[40,41,44,45] Adding methyl acrylate (MA) to the growing polyolefin chain suppressed further coordination insertion of ethylene and formed a six-membered macrochelate (intermediate 1B). In the presence of acetonitrile (MeCN) and under blue light irradiation, the macroradical at the alpha or gamma position to the carbonyl was generated.[37] The radical trapping with TEMPO allowed the preparation of macroinitiator M1 and M2 species, installing terminal α-bromoisobutyrate functionality at the polyolefin chain ends (Figure S2, Supporting Information).[37,41]

2.1. Optimizing PMA Synthesis via SARA ATRP in Chlorobenzene

Prior to analyzing the activity of TEMPO-Br captured polyolefin-based macroinitiators, model reactions with model ATRP initiators were carried out to optimize the reaction conditions. Ethyl α-bromoisobutyrate, EBiB, was used as the analogue to the ester-linked tertiary-bromide terminated macroinitiator. Chlorobenzene was chosen as the solvent because both the polyolefin and polyacrylate blocks are soluble in chlorobenzene.[40] For ATRP techniques, SARA ATRP was selected (Figure S3, Supporting Information). The metallic Cu^0 in SARA ATRP previously showed high polymerization efficiencies as well as low dispersities.[30] Furthermore, SARA ATRP prevents the formation of additional radicals in the catalyst reduction process, which may occur during photoATRP and ICAR ATRP.[31]

As demonstrated in **Figure 2**A, methyl acrylate was homopolymerized via SARA ATRP in chlorobenzene by using EBiB as the initiator. Following the selection of appropriate solvent, initiator, and ATRP technique, three ligands commonly used for ATRP: *N,N,N′,N″,N″*-pentamethyldiethylenetriamine (PMDETA),[46] tris(2-pyridylmethyl)amine (TPMA), and tris[2-(dimethylamino)ethyl]amine (Me_6TREN) were compared (Figure 2B–D). When SARA ATRP of methyl acrylate was conducted in chlorobenzene, Me_6TREN yielded polymers with the lowest dispersity (1.07) and the highest monomer conversions (79%). Using Me_6TREN as the ligand, poly(methyl acrylate) and poly(*n*-butyl acrylate) were synthesized to ensure the applicability of the experimental condition with polyacrylate with a range of glass transition temperatures, T_g (Figure 2E). The model experiments using the initiator analogue showed unimodal polyacrylate peak in GPC traces and successful conversion of monomer in a controlled fashion.

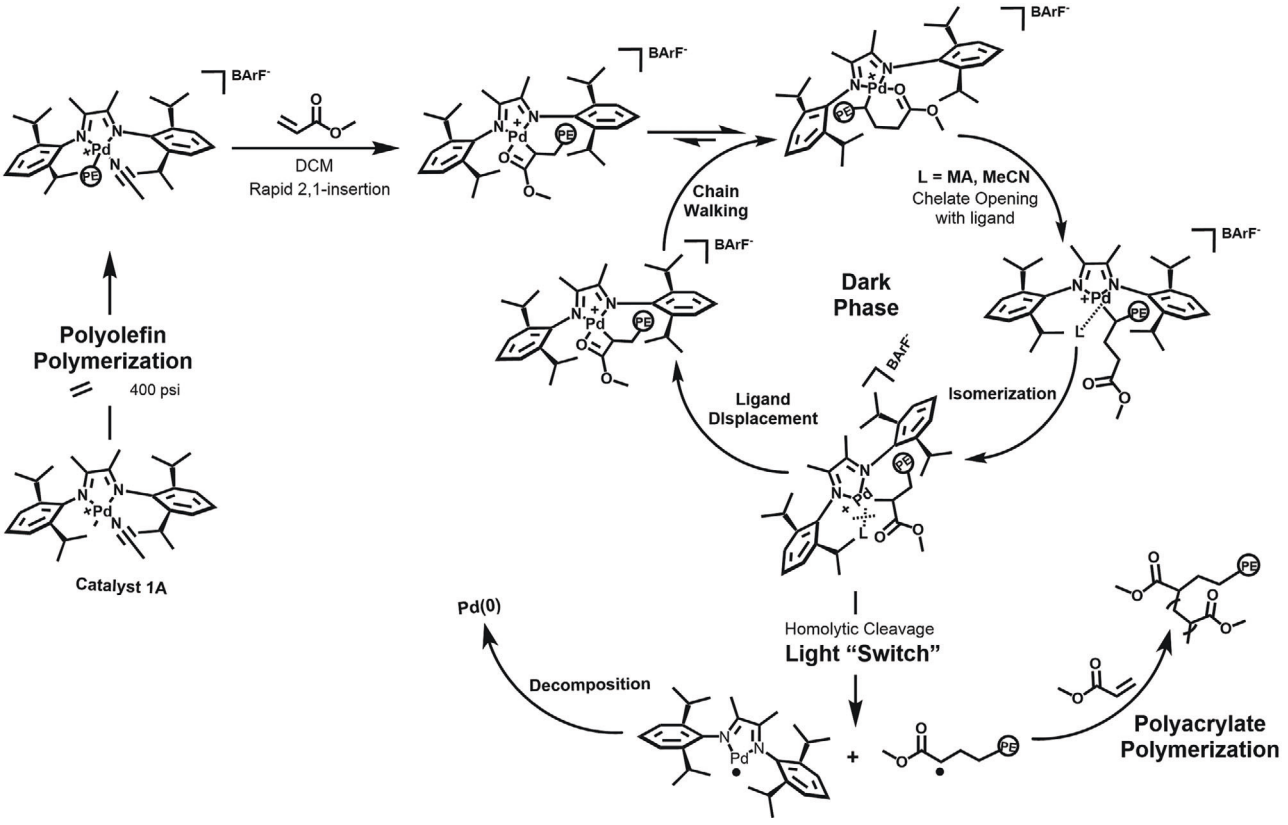

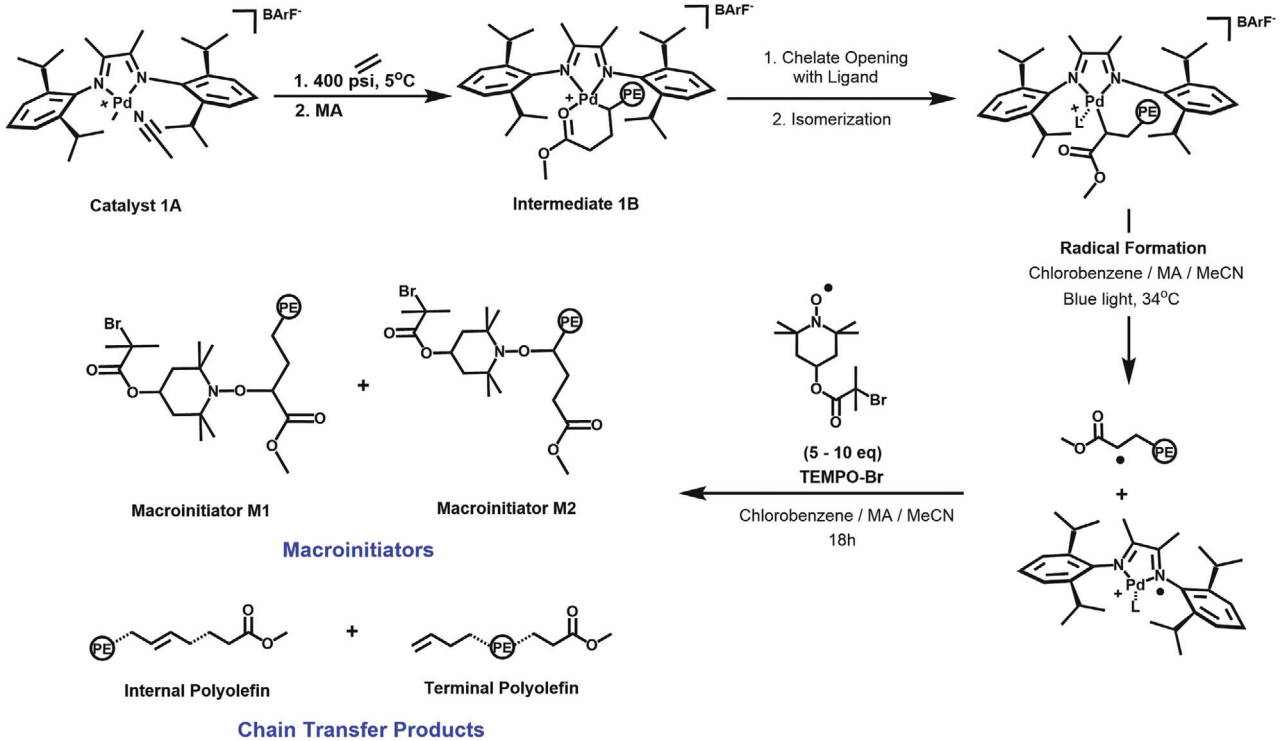

Figure 1. Synthetic scheme of the PO-based ATRP initiator via MILRad. (Top) Targeted synthetic scheme to prepare macroinitiator via conventional MILRad, with free radical polymerization of methyl acrylate. (Bottom) Preparation of polyethylene macroinitiator via tandem living insertion-based MILRad, involving nitroxide group-containing TEMPO.[41] Modified from the previous paper published by Harth et al.[41] 2022, Wiley-VCH. $BArF^-$: Tetrakis[3,5-bis(trifluoromethyl)phenyl]borate.

Kinetic experiments were conducted to provide insights into the rate and molecular weight/dispersity progression during the polymerization (Figure S3, Supporting Information). The monomer conversion and molecular weight evolution were examined from 0 to 20 h (**Figure 3**). For the polymerization of MA with Me_6TREN as the ligand and EBiB as the initiator analogue (Figure 3A), linear semilogarithmic monomer conversion with time was observed (Figure 3B). Unimodal peaks in GPC traces at various time points indicated a controlled polymerization process (Figure 3C). Finally, a linear evolution of molecular weights with conversion was observed. A good match between theoretical and experimental molecular weights as well as low dispersity indicated high initiation efficiency and well-controlled ATRP (Figure 3D).

Relatively slow polymerization was likely due to the low polarity of the chlorobenzene, resulting in low K_{ATRP},[47] previous stud-

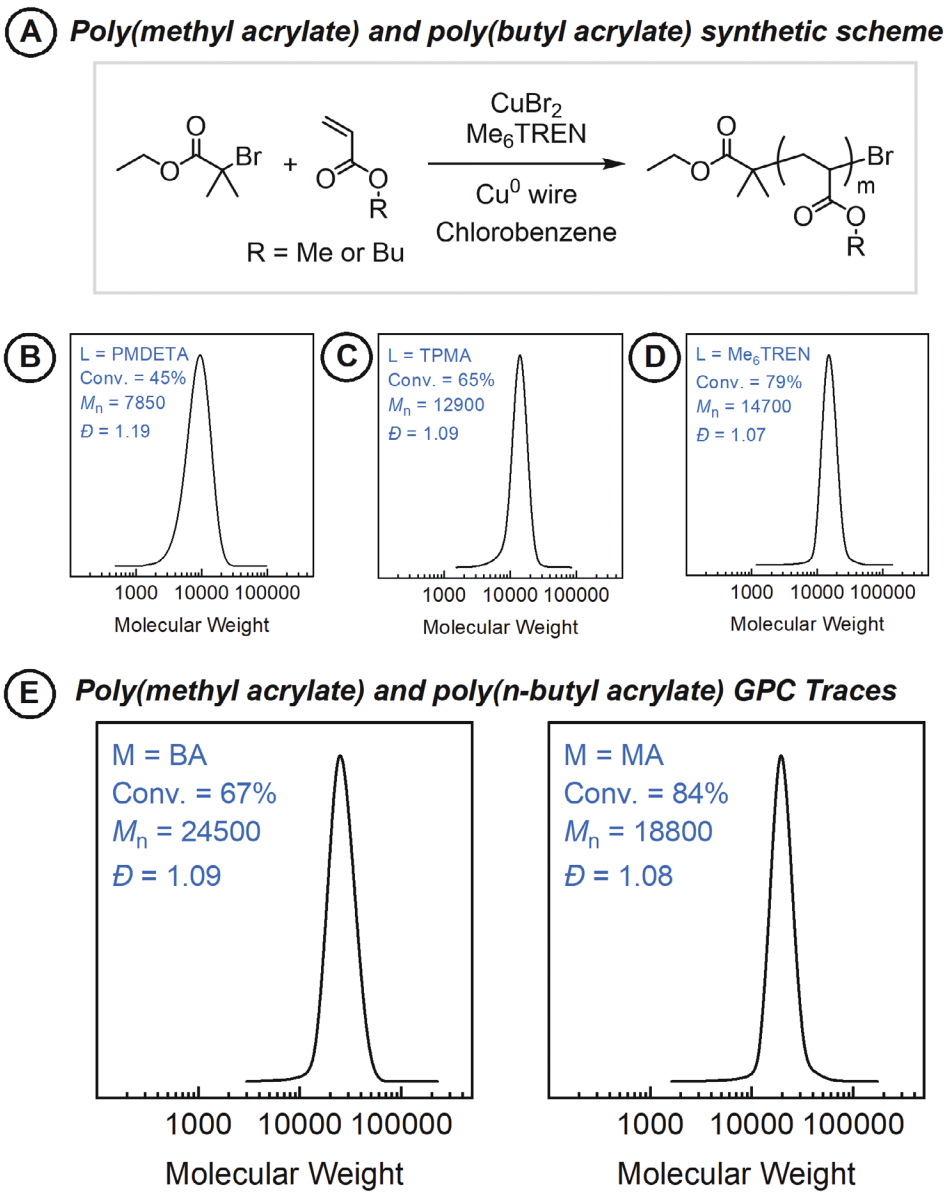

Figure 2. A) PMA and PnBA synthetic scheme. Reaction conditions = [MA]/[EBiB]/[$CuBr_2$]/[L] = 200/1/0.04/0.24 in chlorobenzene (2 vol% MeCN) at room temperature (r.t.). B) THF GPC trace, ligand = PMDETA (*N*,*N*,*N*′,*N*″,*N*″-pentamethyldiethylenetriamine). C) THF GPC traces, ligand = TPMA (tris(2-pyridylmethyl)amine). D) THF GPC traces, ligand = Me_6TREN (tris[2-(dimethylamino)ethyl] amine). E) THF GPC traces of PMA and PBA homopolymer. Reaction condition: [MA]/[EBiB]/[$CuBr_2$]/[Me_6TREN] = 300/1/0.04/0.3 in chlorobenzene (2 vol% MeCN) at r.t.

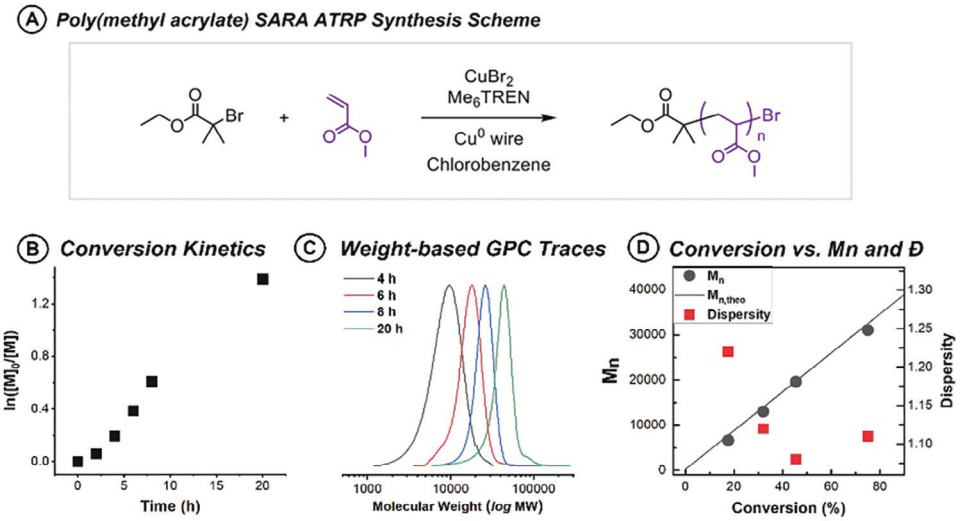

Figure 3. Kinetic data for poly(methyl acrylate) synthesis via SARA ATRP in chlorobenzene. Reaction condition: [MA]/[EBiB]/[$CuBr_2$]/[Me_6TREN] = 500/1/0.04/0.6 in chlorobenzene (with 2 vol% MeCN) with Cu^0 wire at room temperature.[MA] = 3.7 M. A) Polymerization Scheme. B) Polymerization kinetics pattern represented via time versus $\ln([M]_0/[M])$. C) Weight-based THF GPC traces. D) Polymer molar mass and dispersity as a function of conversion.

ies indicated that the solvent with higher polarity contributes to the higher rate of activation for ATRP.[48] A relatively low dielectric constant ($\epsilon = 5.62$) of chlorobenzene possibly contributed to the lower rate of polymerization. Despite low polarity, chlorobenzene was necessary because it dissolves both the polyolefin and polyacrylate block. Previous SARA ATRP polymerizations in nonpolar solvents such as toluene ($\epsilon = 2.38$) showed the formation of well-defined polymers.[49]

2.2. Improving Functionalization Efficiency via Radical Trapping for MILRad Approach

Applying the conditions used for the model reaction outlined in Figure 3, block copolymerization of PE-*b*-PMA was attempted. The preparation of the PE-based macroinitiator via MILRad followed the strategy outlined in Figure 1. Using the PE-based macroinitiator, SARA ATRP in chlorobenzene was carried out for the polymerization of methyl acrylates (**Figure** 4A, Detailed procedure of the synthesis is outlined in Figure S4, Supporting Information).

The peak at 0 h reflects the molar mass of the initial polyethylene-based macroinitiator, ≈10 000 g mol^{-1}. Following 2 h of polymerization, an increase in dispersity was observed from 1.03 to 1.10 (Figure 4B). Furthermore, bimodality began to appear from the sample obtained in 2 h. For the following samples obtained at 5, 8, and 12 h, a clear separation of two peaks was observed. The peaks at low molecular weight remained aligned with the 0 h sample, whereas the peaks at higher molecular weight showed a continuous increase in molecular weight from 2 to 22 h (Figure 4B).

The bimodal traces indicated a fraction of the polyethylene chain remained uninitiated throughout the polymerization. However, linear semilogarithmic monomer conversion with time was observed, indicating continuous conversion up to ≈40% at 12 h (Figure 4C). Furthermore, a good match between the theoretical molecular weight of BCP ($M_{n,th}$ based on 57% functionalization) and the GPC-chromatogram detected molecular weight of BCP (M_n) was observed (Figure 4D). Due to the presence of two peaks, the total dispersity showed a gradual increase. However, the dispersity of the peak at higher MW remained below 1.07 throughout the polymerization (Figure 4D, triangles). These results indicated a well-controlled polymerization of the functionalized polyethylenes, whereas a portion of the chains remained uninitiated.

To investigate the ratio of the initiated polyethylene chains, weight-based original GPC chromatograms were converted to number-based values by dividing the respective refractive index (RI) signal by molecular weight (MW) (Figure 4E). The normalized RI/MW peaks at different time points were deconvoluted and fitted to two Gaussian peaks to compare the relative ratio of area under the BCP peak (A_{BCP}) and the MI peak (A_{MI}). The deconvoluted block copolymer peaks were plotted in Figure 4F. Unimodal peaks with a gradual decrease in elution volume were observed from 0 to 12 h, indicating controlled polymerization of the functionalized macroinitiators (Detailed deconvolution methods outlined in Figure S6, Supporting Information).

The relative area ratios, $A_{BCP}/(A_{BCP} + A_{MI})$, for number-based GPC traces were plotted in Figure 4G as black circles. The ratios were adjusted with dn/dc_{BCP} at different time points (Figure 4G). The BCP yields were ≈57% throughout the polymerization up to 12 h. (Detailed dn/dc calculation methods are outlined in Figure S7, Supporting Information).

Thus, 57% of the initial PE chains were successfully initiated and yielded well-defined block copolymers. However, the remaining 43% of the chains were uninitiated. To investigate the cause of such a phenomenon, a detailed ^{1}H NMR analysis was carried out to determine the efficiency of polyethylene functionalization via radical trapping.

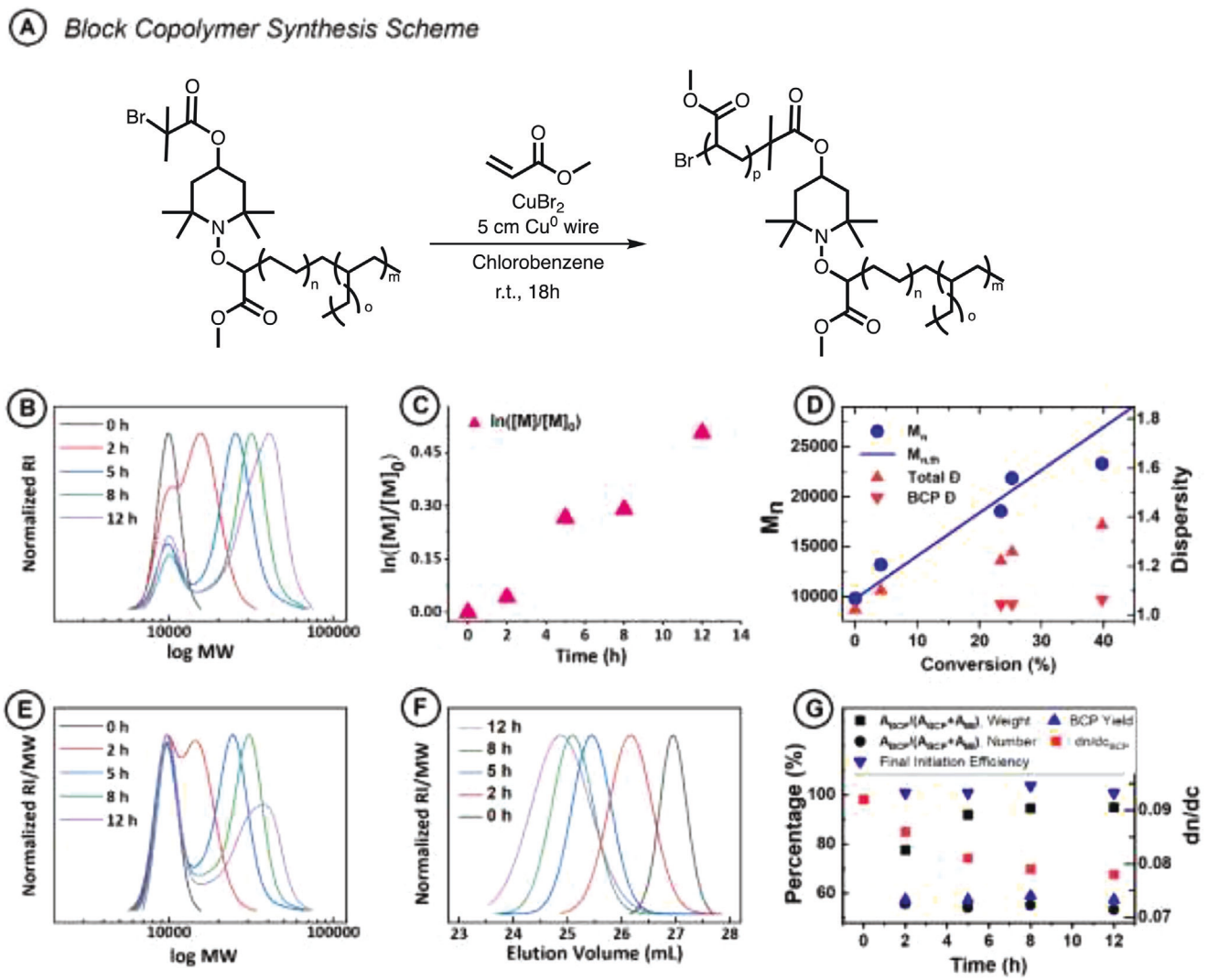

Figure 4. Reaction Condition: [MA]/[PE^{Σ}_{57}]/[$CuBr_2$]/[Me_6TREN] = 1:500:0.04:0.06 in chlorobenzene at r.t. Cu^0 wire = 5 cm, all reagents deoxygenated with N_2 prior to polymerization. A) Reaction Scheme. B) Weight-based THF GPC traces. C) Polymerization kinetics pattern represented via time versus $\ln([M]_0/[M])$. D) M_n and dispersity pattern at various points of conversion. E) Number-based THF GPC traces. F) Deconvoluted BCP peaks. G) Initiation efficiency and BCP yield, and peak area curve ratio of BCP and d*n*/d*c* of block copolymer at varying time points.

Indeed, ^{1}H NMR analysis of the prepared PE-based macroinitiator suggested a mixture of products comprising of the desired PE-TEMPO-Br as well as nonfunctionalized unsaturated PE with a single unit of MA at the chain end, which was formed as a result of β-hydride elimination and subsequent chain termination. The molar ratio of PE-TEMPO-Br to unsaturated PE was 57 to 43, which is in good agreement with the calculated molar ratio of BCP to residual PE from GPC traces (**Figure 5**, top). Specifically, vinyl protons of both terminal (D, 1H) and internal (A,A′, 2H) olefins can be distinctively observed at 5.8 and 5.4 ppm, respectively. On the other hand, PE-TEMPO-Br can be detected via the methine proton B (1H) at 5.0 ppm, and the major α-product is characterized by the methine proton C at 4.2 ppm. However, it is notable that the signal of B overlapped with the vinyl proton E,E′ of the terminal olefin. Therefore, the yield of PE-TEMPO-Br or the functionalization efficiency was determined as shown in Equation (1), in which I_X are the values of integrated NMR peaks.

$$\text{Functionalization Efficiency} = \frac{I_{B,E,E'} - 2I_D}{I_D + 2I_{A,A'} + (I_{B,E,E'} - 2I_D)} \quad (1)$$

For the analysis of this polymer sample, using the values of $I_{B,E,E'}$ (2.35), I_D (0.29), and $I_{A,A'}$ (2) into the formula will result in the functionalization efficiency of 57%. Additionally, due to the inherent deviation in the isolated yield of the reaction, which was obtained after column chromatography, the overall efficiency for this reaction was within the range of 53% ± 4%.

Based on the mechanistic understanding of the MILRad process, faster homolytic cleavage of the Pd—C bond is crucial to minimize the β-hydride elimination. Such an elimination reaction produces undesirable unsaturated PE chains and

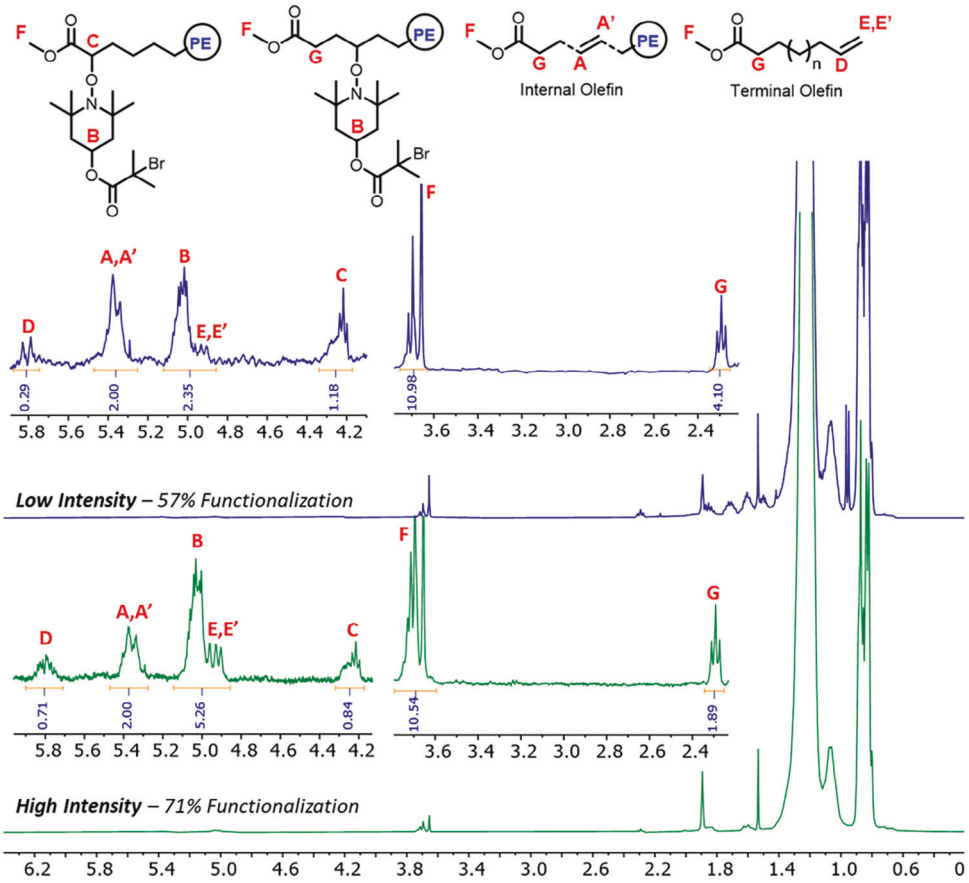

Figure 5. Analyzed ^{1}H NMR spectra (Scan numbers = 256, $CDCl_3$, 25 °C) of the macroinitiators post-functionalization following the purification process; (top) low-intensity light (I = 0.5 mW cm^{-2}), 57% functionalization, (bottom) high-intensity light (I = 200 mW cm^{-2}), 71% functionalization.

decreases the trapping efficiency of PE macroradicals with nitroxides.[32,40,42] Thus, it was hypothesized that stronger light intensity should result in a more pronounced labilization of the Pd—C bond, which would then undergo faster bond homolysis. As a result, the experimental set-up was further optimized by upgrading the original LED light strip with a low light intensity (I) of 0.5 mW cm^{-2} to the state-of-the-art Kessil Lamp, which generates significantly more intense light and energy for the reaction. Our hypothesis correlated positively with the experimental data as the functionalization efficiency improved from 57% (I = 0.5 mW cm^{-2}) to 68% (I = 100 mW cm^{-2}) to 71% (I = 200 mW cm^{-2}). Specifically, the characteristic methine proton B of PE-TEMPO-Br showed an increase of integrated value $I_{B,E,E'}$ from 2.35 to 5.26 relative to the normalized $I_{A,A'}$ value of 2.0, which corresponded to a functionalization efficiency of 71%, as the light intensity was increased from 0.5 to 200 mW cm^{-2} (Figure 5, bottom). Despite different light intensities, the 456 nm light wavelength used for the functionalization remained the same. The wavelength of the light affects the metal–carbon bond cleavage to a certain degree. Different wavelengths have been studied previously to produce macroradicals for a subsequent free radical polymerization but not for the functionalization efficiency. For example, UV–vis was also successful in the metal–carbon bond cleavage and subsequent polymerization. Green light resulted in a lower polymer yield. The summary of light intensity, light source, and the relative functionalization efficiency are summarized in Table S1 (Supporting Information) (Medium intensity light NMR traces shown in Figure S7, Supporting Information).

Our hypothesis of modulating the light intensity was corroborated by a recent study by Poli et al.[37] that provided deeper insights into the process of radical trapping as well as a possible explanation of the limited functionalization efficiency. Density functional theory computation, showed that the unsaturated unfunctionalized PE was formed via the pathway of β-hydride elimination. In this study, a new mechanistic pathway was proposed in which the Pd(II)-hydride species generated via β-hydride elimination can act as a radical quencher to form saturated unfunctionalized PE (**Figure** 6A). Thus, polyethylene macroradical must undergo cage escape, depending on the reaction conditions. To elaborate, successful radical trapping during functionalization hinged upon maximizing cage escape and minimizing β-hydride elimination. Higher light intensity should increase the amount of radical species and their cage escape. This aligned with our experimental data as the higher light intensity indeed resulted in a higher ratio of macroradical (71%) to be trapped by TEMPO complexes (Figure 5).

A positive correlation between light intensity and the functionalization efficiency indicated that increased light intensity resulted in a faster cleavage of Pd—C bond and higher concentration of PE macroradicals. Thus, to further increase the

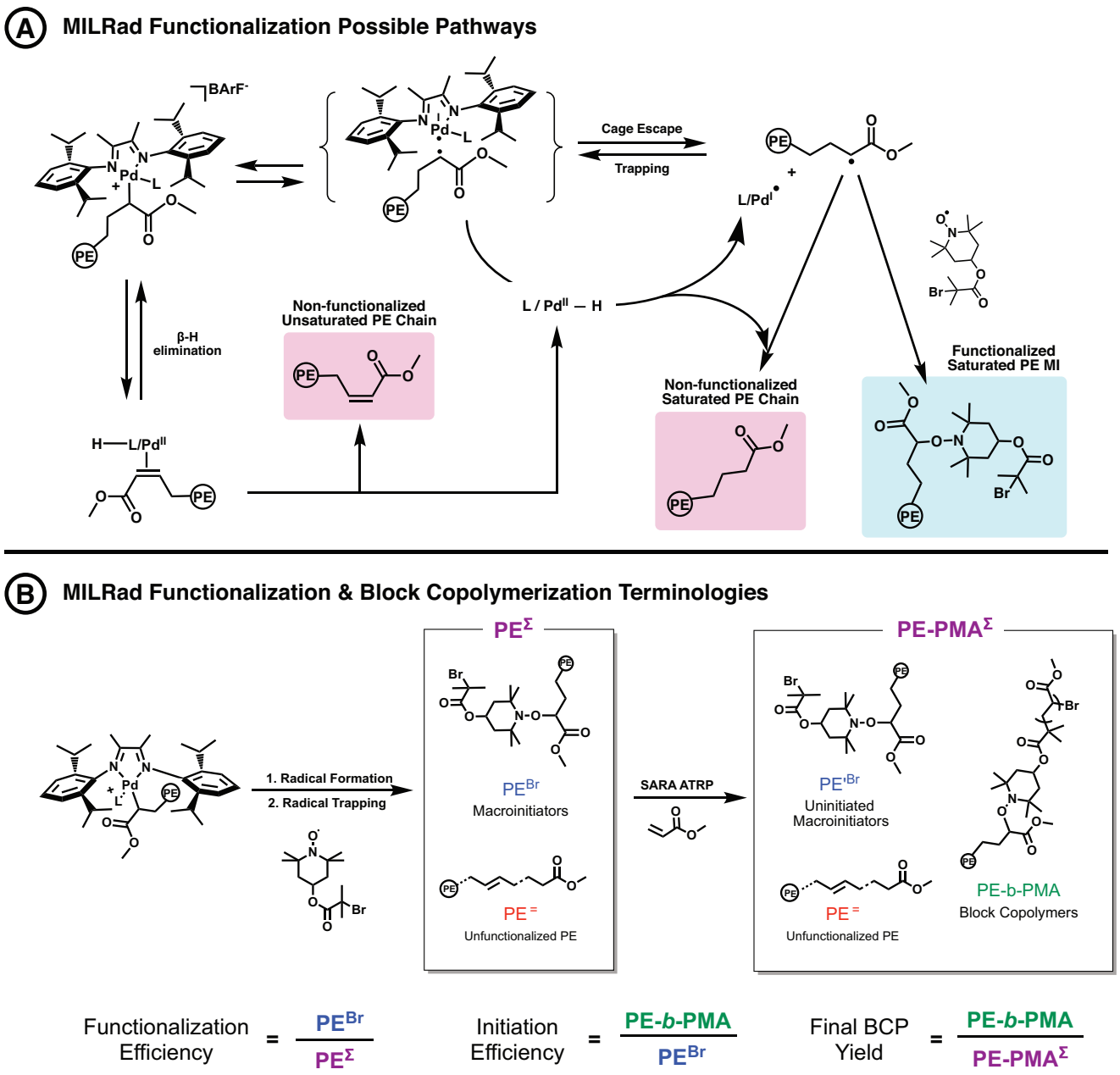

Figure 6. (Top) Proposed pathways of non-functionalized PE chain formation during MILRad synthesis, following the β-hydride elimination pathway. Modified from the ref. [37] 2023, American Chemical Society. (Bottom) Products following radical trapping and block copolymerization. Macroinitiator M1 represents both macroinitiator (M1 and M2), and unfunctionalized PE represents both internal and terminal unsaturated polyethylene.

functionalization efficiency for future studies, efforts should be concerted on minimizing the amount of β-hydride elimination, which should result in a lower amount of unfunctionalized polyolefin.

Figure 6B illustrates the terminology used in this study to clarify the product following each step of the MILRad strategy. PE^{Br} refers to the macroinitiators (functionalized polyolefin chains) following the successful radical trapping. On the other hand, $PE^{=}$ refers to the internal and terminal unsaturated polyethylene.[37] Due to the minuscule differences in the end groups, it is challenging to separate PE^{Br} from $PE^{=}$ by chromatography or solubility differences. Thus, the mixture of PE^{Br} and $PE^{=}$, heretofore referred to as PE^{Σ}, was used for block copolymerization.

Starting from PE^{Σ} as the macroinitiator species for block copolymerization, $PE^{=}$ remained unreactive due to the absence of initiable tertiary halide chain end functionality, but PE^{Br} was initiated and extended to form PE-*b*-PMA. Functionalized uninitiated macroinitiator is referred to as PE'^{Br}. Thus, following the second block extension, $PE^{=}$, PE'^{Br}, and PE-*b*-PMA should coexist in the final sample. Such a product is referred to as PE-PMA^{Σ}. All polyethylene species were characterized by number

Table 1. The yield of block copolymers and initiation efficiency using various PO macroinitiators.

#	Light Intensity	[I]:[M]	$[M]_0$	Cat:Lig	Time [h]	Conv. [%]	$(\frac{dn}{dc})_{BCP}$	Final BCP Yield [%]	BCP $Đ$	Initiation eff. [%]
1	Low Intensity[a] (53% ± 4%)	1:800	6.8 M	0.1:0.0	18	1	0.092	0	—	0
2		1:400	5.2 M	0.1:0.6	19.5	30	0.072	49.4	1.04	99 ± 1
3		1:500	3.2 M	0.04:0.6	8	25	0.079	57.4	1.05	104 ± 6
4	Medium Intensity (68%)	1:600	5.2 M	0.04:0.6	18	38	0.079	65.6	1.09	97 ± 1
5		1:1000	5.2 M	0.04:0.6	18	54	0.067	68.1	1.14	100 ± 4
6		1:1300	5.2 M	0.04:0.6	18	63	0.066	68.3	1.17	100 ± 6
7	High Intensity (71%)	1:800	2.0 M	0.1:0.6	17	51	0.076	70.8	1.14	100 ± 2
8[b]		1:1300	5.5 M	0.1:0.6	18	77	0.072	72.0	1.07	101 ± 1

MA was monomer for the second block using SARA ATRP. Cu^0 wire L = 5 cm, D = 0.5 mm; [a] Entry 1–2: 50% functionalized PE^{Σ}; Entry 3: 57% functionalized PE^{Σ}; [b] Experiment conducted in 40 °C, others at 25 °C.

and weight distributions. Functionalization efficiency measures the ratio of the functionalized chain to the total PE chain. Initiation efficiency is defined as the ratio of the block copolymer chain to the initial macroinitiator chain number. Finally, BCP yield represents the number of block copolymer chains to the total number of PE chains following the block copolymerization (Figure 6B).

2.3. Synthesis of PE-Polar BCP with Near-Quantitative Initiation Efficiency

Using $\mathbf{PE^{\Sigma}}$ with different degrees of functionalization, polyolefin-*block*-poly(methyl acrylate) copolymers were synthesized. The level of functionalization varied for low-intensity light: 50% and 57%. For the medium intensity light prepared PE^{Σ}, the functionalization efficiency reached 68%. For high-intensity light-prepared PE^{Σ}, the level of functionalization reached 71%. In most cases, quantitative or near-quantitative initiation of the macroinitiators was observed. The final BCP yield and initiation efficiency are presented in **Table 1**.

The final block copolymer yield and the initiation efficiency were calculated based on the formula presented in Figure 6. Final BCP yield measured the percentage of PE-*b*-PMA copolymer chains among all polymer chains present post-ATRP. The initiation efficiency measured the percentage of macroinitiators that underwent the block extension. Similar to the analysis presented in Figure 4, the BCP yield was obtained by converting the weight-based GPC chromatogram to number-based GPC chromatogram, followed by deconvolution and adjustment using d*n*/d*c* value (Detailed steps outlined in Figure S6, Supporting Information). The initiation efficiency was calculated by dividing final BCP yield by functionalization efficiency (Figure 6B).

The block copolymers shown from entries 1 to 2 were synthesized with $\mathbf{PE^{\Sigma}}_{50}$. For entry 1, the polymerization was conducted without ligand, which resulted in 1% conversion and almost no observable blocking efficiency from GPC traces (Figure S8, Supporting Information). This indicated the necessity of ligands in the SARA ATRP process (Table 1, Entry 1). When catalysts and ligands were present, almost quantitative initiation efficiencies were observed, as shown in entry 2 (Figure S9, Supporting Information). Entry 3 utilized $\mathbf{PE^{\Sigma}}_{57}$. Despite shorter reaction time, almost quantitative initiation efficiency was observed (Figure S10, Supporting Information). This indicated that the initiation of the macroinitiators took place in the relatively early stages of the polymerization. Regardless of the conversion, near-quantitative initiation efficiency of over 98% was observed for all entries using low-intensity light prepared $\mathbf{PE^{\Sigma}}$.

Entries 4 to 6 utilized medium-intensity light prepared $\mathbf{PE^{\Sigma}}$. Entries from 4–6 indicated that the increase in the monomer-to-initiator ratio resulted in faster polymerization. Entry 4, with the 600:1 monomer-to-initiator ratio, showed 38% conversion at 18 h (Figure S11, Supporting Information). However, the conversion increased to 54% for entry 5, with 800:1 monomer-to-initiator ratio (Figure S12, Supporting Information). For entry 6, with 1300:1 monomer-to-initiator ratio, 63% conversion was observed (Figure S13, Supporting Information). Despite the differences in conversion, all of the macroinitiators demonstrated near-quantitative initiation efficiency, with the final BCP yield similar to that of functionalization efficiency.

The block copolymers shown from entries 7 and 8 were synthesized with high-intensity light prepared $\mathbf{PE^{\Sigma}}_{71}$. Despite a high monomer-to-initiator ratio of 800:1, the monomer concentration was 2.0 M, which may have contributed to a lower conversion reached at 17 h (Figure S14, Supporting Information). Entry 8 was performed at an increased temperature of 40 °C. Higher temperature, combined with a high monomer-to-initiator ratio (1300:1), possibly contributed to the highest level of conversion (77%) in 18 h. For both entries, near quantitative initiations were observed (Figure S15, Supporting Information). Entry 8 indicated that the increased temperature did not negatively affect the initiation efficiency of the macroinitiators.

The relative area ratios, $A_{BCP}/(A_{BCP} + A_{MI})$, for number-based GPC traces are plotted in **Figure 7D** as black circles. The ratios were adjusted with dn/dc_{BCP} at different time points. The BCP yields were ≈71% throughout the polymerization up to 18 h. Almost quantitative initiation was observed throughout the samples taken from 2 to 18 h (Figure 7D, green hexagon). For the 2 h sample, the height of the PE^{Σ} peak is slightly higher than the ones compared to 6, 16, and 18 h samples. However, as the 2 h sample has a wider block copolymer peak, almost quantitative initiation was observed for the 2 h sample as well (Figure 7C).

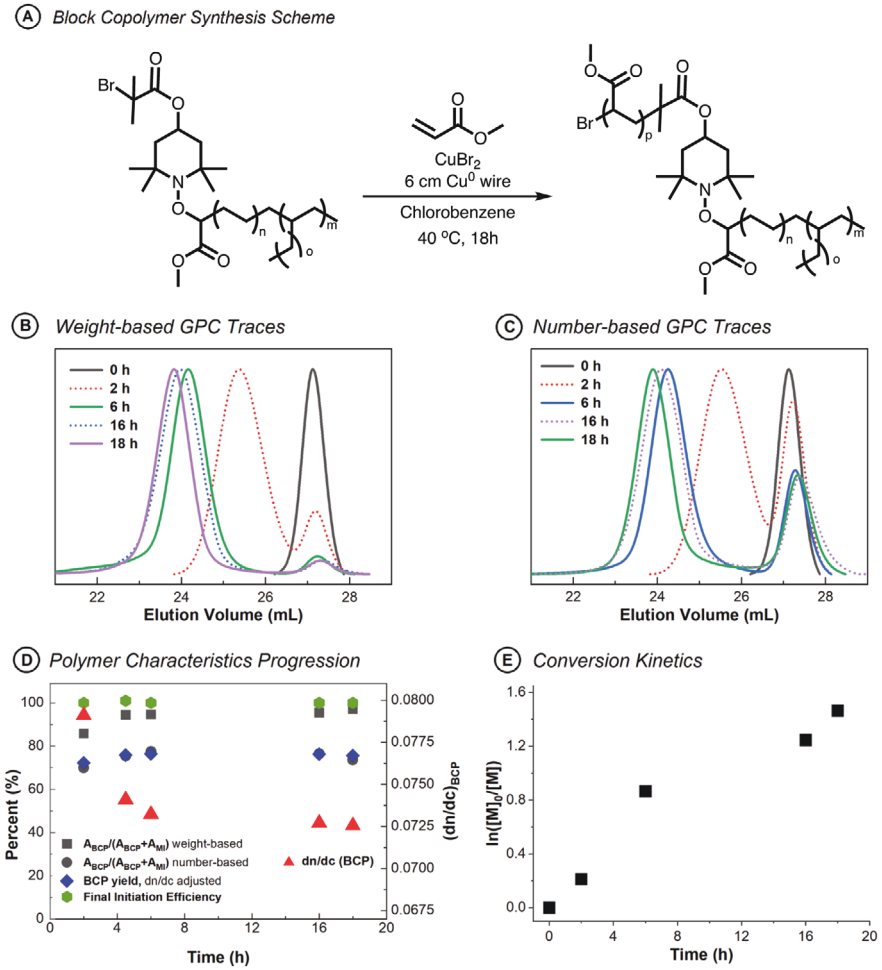

Figure 7. Reaction conditions: [MA]/[PE$^{\Sigma}_{71}$]/[$CuBr_2$]/[Me_6TREN] = 1300/1/0.1/0.6 in chlorobenzene (with 2% DMF) in the presence of Cu^0 wire at 40 °C. [MA] = 3.4 M, PE-PE$^{\Sigma}_{71}$ = 155 mg ($M_{n,GPC}$ = 10 600 g mol^{-1}, $M_{n,NMR}$ = 9100 g mol^{-1}). A) Block copolymer synthesis scheme. B) Weight-based distribution of the GPC traces as a function of elution volume. C) Number-based distribution of the GPC traces. D) Initiation efficiency and BCP yield, and peak area curve ratio of the BCP and d*n*/d*c*. E) Polymerization kinetics pattern represented via time versus ln([M]$_0$/[M]).

Linear semilogarithmic kinetic plots indicated well-controlled ATRP with fast initiation (Figure 7E). High chain end fidelity of the macroinitiators was demonstrated from the quantitative initiation of the PE^{Br}. This indicated that MILRad-prepared macroinitiators are highly compatible with SARA ATRP, and all functionalized polyethylenes were initiated despite the presence of unfunctionalized polyethylene chains. Furthermore, to confirm the successful synthesis of block copolymers, diffusion ordered spectroscopy was carried out. The PE-*b*-PMA block copolymer synthesized using **PE$^{\Sigma}_{68}$**, presented as entry 4 of Table 1 was used for the analysis. The purified PE-*b*-PMA sample showed a single resonance in which the signals of PE (1.26–0.0 ppm) and PMA (3.65 ppm) were aligned and confirmed the formation of block copolymers (Figure S17, Supporting Information).

To further examine the range of applicability of the MILRad approach, a polyhexene (PH)-based macroinitiator was prepared and examined. PH$^{\Sigma}_{50}$ was utilized for the synthesis of PH-*block*-PMA. Reaction conditions used for the preparation of PE-*b*-PMA shown in Figure 4 were used. Both the weight-based and number-based GPC traces indicated the presence of bimodal peaks, each correlated to uninitiated PH$^{=}$ in PH$^{\Sigma}_{50}$ and growing PH-*block*-PMA chain. The peaks at higher M_n showed a gradual increase in molecular weight with time, indicating the controlled polymerization of the PMA block. Almost quantitative initiation was observed for samples taken at 6, 8, 10, and 22 h. Conversion reached ≈45% at 22 h. Linear semilogarithmic kinetic plots, along with continuous polymer growth observed in GPC traces, indicated successful extension of the PMA block via SARA ATRP (Figure S16, Supporting Information).

3. Conclusion

This study examined the efficiency of the synthesis of polyolefin-*block*-polyacrylate copolymer via the MILRad functionalization approach. Higher light intensity in the radical trapping step resulted in higher functionalization efficiency, as determined by the NMR analysis of the chain end structures. Radical trapping efficiency—measured by the percent of α-bromoisobutyrate functional group installed on polyolefins—increased from ≈50% to above 70%. Near quantitative initiation of macroinitia-

tor chains with tertiary halide functionality was observed. Despite the presence of unfunctionalized polyolefin chains, controlled polymerization of acrylates was observed. The block copolymer yield and the functionalization efficiency aligned closely. Although PE-*b*-PMA block copolymers were the most extensively synthesized and studied in this study, the successful preparation of PH-*b*-PMA indicated that the MILRad approach can be applied to other olefinic monomers as the first block. As the initiation efficiency was almost quantitative for MILRad-prepared PE^{Br}, improvements in the radical trapping efficiency should increase the block copolymer yield. Successful synthesis of polyolefin–polar block copolymers may allow access to polymer self-assembly, a unique characteristic associated with BCPs.[50–52]

The improvement of radical trapping efficiency with stronger light intensity correlated with the recent computational findings by Poli et al.[37] Future efforts will focus on diminishing the amount of β-hydride elimination by varying light wavelengths and intensity, functionalization time, solvent, and temperature. As the bottleneck of the MILRad approach lies at the low trapping efficiencies of the radical formed from homolytic cleavage, an approach that bypasses this step will be studied along with MILRad. PACE,[3] polyolefin active ester exchange, utilizes a similar concept of conjoining coordination–insertion polymerization and RDRP, albeit without the need for the homolytic cleavage step. Finally, more accessible transition metals, such as nickel, may be used as the PACE and MILRad catalysts, rendering such strategies more industrially attractive and widely available.[12,53–55] The investigation to broaden the applicability and deepen the understanding of the mechanism of MILRad could allow the preparation of polyolefin–polar block copolymers in higher yield.

Supporting Information

Supporting Information is available from the Wiley Online Library or from the author.

Acknowledgements

The authors gratefully acknowledge the Robert A. Welch Foundation for funding (H-E-0041 and E-2066-202110327 (E.H)) and acknowledge the National Science Foundation (CHEM-2108576 (E.H.) and CHE-2108901 (K.M.)) for supporting this work.

Conflict of Interest

The authors declare no conflict of interest.

Data Availability Statement

The data that support the findings of this study are available from the corresponding author upon reasonable request.

Keywords

atom transfer radical polymerization, block copolymers, copolymerization, metal–organic insertion light-initiated radical, polyolefins

Received: November 22, 2023
Revised: December 19, 2023
Published online: January 9, 2024

[1] S. D. Ittel, L. K. Johnson, M. Brookhart, *Chem. Rev.* **2000**, *100*, 1169.
[2] W. Kaminsky, *Macromol. Chem. Phys.* **2008**, *209*, 459.
[3] H. Dau, E. Tsogtgerel, K. Matyjaszewski, E. Harth, *Angew. Chem., Int. Ed.* **2022**, *61*, e202205931.
[4] G. Natta, I. Pasquon, in *Advances in Catalysis* (Eds: D. D. Eley, P. W. Selwood, P. B. Weisz), Academic Press, Cambridge, MA **1959**, pp. 1–66.
[5] K. Ziegler, E. Holzkamp, H. Breil, H. Martin, *Angew. Chem.* **1955**, *67*, 541.
[6] G. Natta, P. Pino, P. Corradini, F. Danusso, E. Mantica, G. Mazzanti, G. Moraglio, *J. Am. Chem. Soc.* **1955**, *77*, 1708.
[7] P. Cossee, *J. Catal.* **1964**, *3*, 80.
[8] W. Kaminsky, *Macromol. Chem. Phys.* **1996**, *197*, 3907.
[9] W. Kaminsky, *J. Chem. Soc., Dalton Trans.* **1998**, 1413.
[10] L. K. Johnson, C. M. Killian, M. Brookhart, *J. Am. Chem. Soc.* **1995**, *117*, 6414.
[11] L. K. Johnson, S. Mecking, M. Brookhart, *J. Am. Chem. Soc.* **1996**, *118*, 267.
[12] C. M. Killian, D. J. Tempel, L. K. Johnson, M. Brookhart, *J. Am. Chem. Soc.* **1996**, *118*, 11664.
[13] K. Matyjaszewski, *Macromolecules* **2012**, *45*, 4015.
[14] K. Matyjaszewski, J. Xia, *Chem. Rev.* **2001**, *101*, 2921.
[15] J.-S. Wang, K. Matyjaszewski, *J. Am. Chem. Soc.* **1995**, *117*, 5614.
[16] N. Corrigan, K. Jung, G. Moad, C. J. Hawker, K. Matyjaszewski, C. Boyer, *Prog. Polym. Sci.* **2020**, *111*, 101311.
[17] D. Konkolewicz, A. J. D. Magenau, S. E. Averick, A. Simakova, H. He, K. Matyjaszewski, *Macromolecules* **2012**, *45*, 4461.
[18] T. G. Ribelli, F. Lorandi, M. Fantin, K. Matyjaszewski, *Macromol. Rapid Commun.* **2019**, *40*, 1800616.
[19] F. Lorandi, M. Fantin, K. Matyjaszewski, *J. Am. Chem. Soc.* **2022**, *144*, 15413.
[20] S. Dadashi-Silab, K. Kim, F. Lorandi, D. J. Schild, M. Fantin, K. Matyjaszewski, *Polym. Chem.* **2022**, *13*, 1059.
[21] S. Dadashi-Silab, K. Matyjaszewski, *ACS Macro Lett.* **2019**, *8*, 1110.
[22] V. Vasu, J.-S. Kim, H.-S. Yu, W. I. Bannerman, M. E. Johnson, A. D. Asandei, *Polym. Chem.* **2018**, *9*, 2389.
[23] N. J. Treat, H. Sprafke, J. W. Kramer, P. G. Clark, B. E. Barton, J. Read de Alaniz, B. P. Fors, C. J. Hawker, *J. Am. Chem. Soc.* **2014**, *136*, 16096.
[24] K. Matyjaszewski, W. Jakubowski, K. Min, W. Tang, J. Huang, W. A. Braunecker, N. V. Tsarevsky, *Proc. Natl. Acad. Sci. USA* **2006**, *103*, 15309.
[25] M. Chen, M. Zhong, J. A. Johnson, *Chem. Rev.* **2016**, *116*, 10167.
[26] D. Konkolewicz, K. Schroder, J. Buback, S. Bernhard, K. Matyjaszewski, *ACS Macro Lett.* **2012**, *1*, 1219.
[27] W. Jakubowski, K. Min, K. Matyjaszewski, *Macromolecules* **2006**, *39*, 39.
[28] W. Jakubowski, K. Matyjaszewski, *Angew. Chem., Int. Ed.* **2006**, *45*, 4482.
[29] D. Konkolewicz, Y. Wang, P. Krys, M. Zhong, A. A. Isse, A. Gennaro, K. Matyjaszewski, *Polym. Chem.* **2014**, *5*, 4409.
[30] D. Konkolewicz, Y. Wang, M. Zhong, P. Krys, A. A. Isse, A. Gennaro, K. Matyjaszewski, *Macromolecules* **2013**, *46*, 8749.
[31] Y. Zhang, Y. Wang, K. Matyjaszewski, *Macromolecules* **2011**, *44*, 683.
[32] A. Keyes, H. E. B. Alhan, U. Ha, Y.-S. Liu, S. K. Smith, T. S. Teets, D. B. Beezer, E. Harth, *Macromolecules* **2018**, *51*, 7224.
[33] C. Zou, G. Si, C. Chen, *Nat. Commun.* **2022**, *13*, 1954.
[34] K. Tanaka, K. Matyjaszewski, *Macromolecules* **2007**, *40*, 5255.
[35] Z. Chen, M. Brookhart, *Acc. Chem. Res.* **2018**, *51*, 1831.
[36] S. Mecking, L. K. Johnson, L. Wang, M. Brookhart, *J. Am. Chem. Soc.* **1998**, *120*, 888.
[37] R. Poli, D. Nguyen, Y.-S. Liu, E. Harth, *Organometallics* **2023**, *42*, 1110.
[38] S. B. Amin, T. J. Marks, *Angew. Chem., Int. Ed.* **2008**, *47*, 2006.
[39] J. Y. Dong, T. C. Chung, *Macromolecules* **2002**, *35*, 1622.

[40] H. Dau, A. Keyes, H. E. B. Alhan, E. Ordonez, E. Tsogtgerel, A. P. Gies, E. Auyeung, Z. Zhou, A. Maity, A. Das, D. C. Powers, D. B. Beezer, E. Harth, *J. Am. Chem. Soc.* **2020**, *142*, 21469.
[41] A. Keyes, H. Dau, K. Matyjaszewski, E. Harth, *Angew. Chem., Int. Ed.* **2022**, *61*, e202112742.
[42] A. Keyes, H. Dau, H. E. B. Alhan, U. Ha, E. Ordonez, G. R. Jones, Y.-S. Liu, E. Tsogtgerel, B. Loftin, Z. Wen, J. I. Wu, D. B. Beezer, E. Harth, *Polym. Chem.* **2019**, *10*, 3040.
[43] R. Briquel, J. Mazzolini, T. L. Bris, O. Boyron, F. Boisson, F. Delolme, F. D'Agosto, C. Boisson, R. Spitz, *Angew. Chem., Int. Ed.* **2008**, *47*, 9311.
[44] A. C. Gottfried, M. Brookhart, *Macromolecules* **2001**, *34*, 1140.
[45] A. C. Gottfried, M. Brookhart, *Macromolecules* **2003**, *36*, 3085.
[46] A. K. Nanda, K. Matyjaszewski, *Macromolecules* **2003**, *36*, 1487.
[47] W. A. Braunecker, N. V. Tsarevsky, A. Gennaro, K. Matyjaszewski, *Macromolecules* **2009**, *42*, 6348.
[48] M. Horn, K. Matyjaszewski, *Macromolecules* **2013**, *46*, 3350.
[49] B. D. Hornby, A. G. West, J. C. Tom, C. Waterson, S. Harrisson, S. Perrier, *Macromol. Rapid Commun.* **2010**, *31*, 1276.
[50] A. N. Le, R. Liang, M. Zhong, *Chemistry* **2019**, *25*, 8177.
[51] B. Charleux, G. Delaittre, J. Rieger, F. D'Agosto, *Macromolecules* **2012**, *45*, 6753.
[52] F. D'Agosto, J. Rieger, M. Lansalot, *Angew. Chem., Int. Ed.* **2020**, *59*, 8368.
[53] K. E. Allen, J. Campos, O. Daugulis, M. Brookhart, *ACS Catal.* **2015**, *5*, 456.
[54] P. Preishuber-Pflugl, M. Brookhart, *Macromolecules* **2002**, *35*, 6074.
[55] Z. Chen, K. E. Allen, P. S. White, O. Daugulis, M. Brookhart, *Organometallics* **2016**, *35*, 1756.

